Isoscalar Giant Resonances in a Relativistic Model

M. L'Huillier and Nguyen Van Giai

Division de Physique Théorique*, Institut de Physique Nucléaire,

F-91406 , Orsay Cedex

PACS numbers : 21.10.Re, 21.60.Jz, 21.90.+f

IPNO/TH 88-45 July 1988

*Laboratoire associé au C.N.R.S

Abstract

Isoscalar giant resonances in finite nuclei are studied in a relativistic Random Phase Approximation (RRPA) approach. The model is self-consistent in the sense that one set of coupling constants generates the Dirac-Hartree single-particle spectrum and the residual particle-hole interaction. The RRPA is used to calculate response functions of multipolarity $L = 0, 2, 3$, and 4 in light and medium nuclei. It is found that monopole and quadrupole modes exhibit a collective character. The peak energies are overestimated, but not as much as one might think if the bulk properties (compression modulus, effective mass) were the only relevant quantities.

1 Introduction

The relativistic approach based on an effective Lagrangian density of interacting nucleon and meson fields has proved to be rather successful in describing ground state properties of nuclear systems. Numerous works have been devoted to the study of infinite matter and finite nuclei in the framework of the relativistic mean field (or Dirac-Hartree) and Dirac-Hartree-Fock approximations [1]. It has been shown, for instance, that within a model containing the four mesons σ, ω, π and ρ where the only adjusted parameters are g_σ, g_ω and m_σ, it is possible to have a satisfactory description of binding energies, charge densities and single-particle spin-orbit splittings of doubly-closed shell nuclei from ^{16}O to ^{208}Pb [2].

It is then natural to extend the relativistic model to the description of nuclear excitations. Among them, giant resonances play a prominent role as they reflect collective nuclear properties originating from coherent superpositions of particle-hole (p-h) configurations. Therefore, a sound microscopic framework should be provided by the relativistic Random Phase Approximation (RRPA). The spirit of such an extension of the relativistic model is similar to that of the non-relativistic, self-consistent RPA studies. Indeed, after the success of various effective Hamiltonians in describing nuclear ground states within the Hartree-Fock approximation, it has been shown that these Hamiltonians also give a good description of giant resonances if one performs RPA calculations where single-particle spectra and residual p-h interaction are generated by the same Hamiltonian [3-5].

In the non-relativistic approach, detailed microscopic RPA calculations, when they are

self-consistent, have a close contact with more global results obtained by sum rule methods [6], so that the two kinds of studies supplement each other nicely. On the other hand, relativistic sum rule methods are not available, and one has to resort to detailed RRPA calculations. However, some connection can be made between RRPA and the predictions from scaling methods applied to the (σ,ω) model, which relate in a simple way the monopole and quadrupole energies to the relativistic Landau parameters [7]. Therefore, we shall compare our results to these predictions.

In this work, we study the isoscalar multipole resonances in doubly-closed shell nuclei by the response function method. For simplicity, we assume that the effective Lagrangian has been determined in such a way that the uncorrelated ground state can be treated in the Dirac-Hartree approximation. Then, it is consistent to keep only the direct contributions to the residual p-h interaction. Thus, the present Dirac-Hartree-RPA (DHRPA) corresponds to the ring approximation, i.e., it sums up only the bubble diagrams. This should be sufficient for our purpose of studying isoscalar modes. If one wishes to calculate isovector modes, one would have to use an effective Lagrangian containing also isovector mesons (π and ρ) and start from an uncorrelated ground state of the Dirac-Hartree-Fock type, in which case it would be necessary to include also exchange diagrams in the RRPA. In the next section, we give the general expressions for calculating the response functions in finite nuclei. Section III explains how calculations are done in practice. The results are discussed in section IV. Our conclusions are summarized in the last section.

2 The DHRPA response function

The derivation of the DHRPA equations, using the Green's function method, has been done by Kurasawa and Suzuki [8] for the case of infinite matter. Here, we only need to give the relevant expressions in the case of finite nuclei.

2.1 The single-particle propagator

In the Dirac-Hartree approximation, the single-particle spectrum is determined by a Dirac equation with the self-consistent self-energy Σ :

$$[\gamma_0 E_\lambda + i\vec{\gamma}.\vec{\nabla} - (M + \Sigma_s(\vec{x})) - \gamma^\mu \Sigma_\mu(\vec{x})]h_\lambda(\vec{x}) = 0 \ , \tag{1}$$

where M is the nucleon mass, λ stands for a set of individual quantum numbers, and (E_λ, h_λ) are the corresponding energy and wave function. The self-energies are local, but they can be different for neutrons and protons. For convenience, we shall distinguish in the notation between occupied Fermi states ($\lambda \equiv a; h_\lambda \equiv f_a; E_\lambda \equiv E_a > 0$), unoccupied Fermi states ($\lambda \equiv A; h_\lambda \equiv f_A; E_\lambda \equiv E_A > 0$) and Dirac sea states ($\lambda \equiv \bar{\alpha}; h_\lambda \equiv g_{\bar{\alpha}}; E_\lambda \equiv E_{\bar{\alpha}} < 0$). This is indicated in Fig.1.

The single-particle Hartree propagator is defined by :

$$G_H^{ij}(\vec{x}, \vec{x}'; t - t') \equiv -i < 0|T(\psi_H^i(\underline{x})\bar{\psi}_H^j(\underline{x}'))|0 > \ , \tag{2}$$

where $i, j = 0, 1, 2, 3, \underline{x} = (t, \vec{x})$, and $|0>$ is the uncorrelated Hartree ground state. Expanding

the Hartree field operators ψ_H on the complete set of h_λ spinors :

$$\psi_H(\underline{x}) = \sum_\lambda h_\lambda(\vec{x}) e^{-iE_\lambda t} a_\lambda \ , \tag{3}$$

where a_λ annihilates a nucleon in state λ, one can calculate the Fourier transform :

$$G_H(\vec{x},\vec{x}';E) = \int_{-\infty}^{+\infty} d\tau e^{iE\tau} G_H(\vec{x},\vec{x}';\tau) \ , \tag{4}$$

and obtain the explicit result :

$$\begin{aligned} G_H(\vec{x},\vec{x}';E) &= \left[\sum_{\alpha=a,A} \frac{f_\alpha(\vec{x})\bar{f}_\alpha(\vec{x}')}{E-E_\alpha+i\eta} + \sum_{\bar{\alpha}} \frac{g_{\bar{\alpha}}(\vec{x})\bar{g}_{\bar{\alpha}}(\vec{x}')}{E-E_{\bar{\alpha}}-i\eta} \right] \\ &+ \left[\sum_a f_a(\vec{x})\bar{f}_a(\vec{x}') \left(\frac{1}{E-E_a-i\eta} - \frac{1}{E-E_a+i\eta} \right) \right] \\ &\equiv G_F(\vec{x},\vec{x}';E) + G_D(\vec{x},\vec{x}';E) \ . \end{aligned} \tag{5}$$

In eq.(5), the first bracket is the Feynman propagator G_F, whereas the second bracket corresponds to the density-dependent part G_D.

2.2 The Hartree polarization operator

Let us introduce general, local one-body operators :

$$P(\underline{x}) \equiv \bar{\psi}_H(\underline{x})\Gamma_P\psi_H(\underline{x}) \ , \ Q(\underline{x}) \equiv \bar{\psi}_H(\underline{x})\Gamma_Q\psi_H(\underline{x}) \ , \tag{6}$$

where Γ_P, Γ_Q are arbitrary 4×4 matrices. Following ref.[8], we can define the unperturbed, or Hartree, correlation function :

$$G_0(P,Q;\vec{x},\vec{x}',t-t') \equiv < 0|T(P(\underline{x})Q(\underline{x}'))|0 > \ . \tag{7}$$

It is easy to express its Fourier transform in terms of the single-particle Hartree propagator given by eq.(5). One finds :

$$\begin{aligned} G_0(P,Q;\vec{x},\vec{x}';E) &\equiv \int_{-\infty}^{+\infty} d\tau e^{iE\tau} G_0(P,Q;\vec{x},\vec{x}';\tau) \\ &= \frac{1}{2\pi}\int_{-\infty}^{+\infty} dE' Tr[\Gamma_P G_H(\vec{x},\vec{x}';E+E')\Gamma_Q G_H(\vec{x}',\vec{x};E')] \ . \end{aligned} \tag{8}$$

Using eq.(5), we can see that G_0 contains terms of the type $G_D G_D, G_D G_F, G_F G_D$ and $G_F G_F$. While the three first terms are finite, the last one which represents most the $N\bar{N}$ excitations gives an infinite contribution. This divergence would be renormalized by adding appropriate counterterms to the Lagrangian [9]. Instead of this very cumbersome procedure, we simply ignore this $G_F G_F$ contribution, similarly to what was done in the case of infinite matter [8]. This is consistent with the fact the Dirac-Hartree self-energy $\sum$ is also calculated without including the infinite contribution of G_F instead of performing the renormalization.

With the above approximation, the Hartree correlation function can be written as :

$$G_0(P,Q;\vec{x},\vec{x}';E) = G_0^+ + G_0^- \ , \tag{9}$$

where

$$\begin{aligned} G_0^+(P,Q;\vec{x},\vec{x}';E) &= i\sum_{aA}\left\{ \frac{[\bar{f}_a(\vec{x})\Gamma_P f_A(\vec{x})][\bar{f}_A(\vec{x}')\Gamma_Q f_a(\vec{x}')]}{E_a - E_A + E + i\eta} \right. \\ &\left. + \frac{[\bar{f}_A(\vec{x})\Gamma_P f_a(\vec{x})][\bar{f}_a(\vec{x}')\Gamma_Q f_A(\vec{x}')]}{E_a - E_A - E + i\eta} \right\} \ , \end{aligned} \tag{10}$$

and a similar expression for G_0^- deduced from (10) by replacing f_A, E_A and $i\eta$ by $g_{\bar{a}}$, $E_{\bar{a}}$ and $-i\eta$, respectively. The G_0^+ term represents p-h excitations where a particle jumps from below to above the Fermi level. On the other hand, the G_0^- term corresponds to $N\bar{N}$ excitations, i.e.

to transitions from a Dirac sea state to an occupied Fermi state and therefore it is violating the Pauli principle. This violation is a consequence of the neglect of the $G_F G_F$ diverging term. In any case, the effect of the Pauli violating terms on the calculated giant resonances is always small (see section III).

We can now introduce the unperturbed, or Hartree, polarization operator [10] :

$$\Pi_0(P,Q;\vec{k},\vec{k}';E) \equiv i\int e^{-i\vec{k}.\vec{x}}G_0(P,Q;\vec{x},\vec{x}';E)e^{i\vec{k}'.\vec{x}'}d^3xd^3x' \ , \tag{11}$$

and its multipole expansion :

$$\Pi_0(P,Q;\vec{k},\vec{k}';E) = \sum_{LM} Y^*_{LM}(\hat{k})\Pi_0^{(L)}(P,Q;k,k';E)Y_{LM}(\hat{k}') \ . \tag{12}$$

The Hartree response function is then given by :

$$R_0(P,Q;k,E) \equiv \frac{1}{\Pi}\Im m\ \Pi_0(P,Q;\vec{k},\vec{k}';E) \ . \tag{13}$$

It is quite easy to obtain an explicit expression for the multipole components of Π_0. Using eqs.(9 - 10), they can be split into :

$$\Pi_0^{(L)} = \Pi_0^{(L)+} + \Pi_0^{(L)-} \ , \tag{14}$$

where

$$\Pi_0^{(L)+}(P,Q;k,k';E) = \frac{(4\pi)^2}{2L+1}\sum_{aA}(-1)^{j_a+j_A}\left\{\frac{<\bar{f}_a||P_L||f_A><\bar{f}_A||Q_L||f_a>}{E_a-E_A+E+i\eta}\right. \tag{15}$$

$$\left.\frac{<\bar{f}_A||P_L||f_a><\bar{f}_a||Q_L||f_A>}{E_a-E_A-E+i\eta}\right\} .$$

In eq.(15), the reduced matrix elements of the multipole components of operators P, Q appear in the numerators, and the sums are over single-particle quantum numbers excluding third components of angular momenta. The expression for $\Pi_0^{(L)-}$ can be deduced from eq.(15) by replacing f_A, E_A and $i\eta$ by $g_{\bar{\alpha}}$, $E_{\bar{\alpha}}$ and $-i\eta$, respectively.

2.3 The RRPA polarization operator

When the effects of residual p-h interaction are taken into account in the ring approximation, the Hartree correlation function G_0 is replaced by the RRPA correlation function G where all disconnected diagrams are excluded. In the isoscalar channel, only σ and ω induced interactions are effective. Making use of nucleon current conservation, the RRPA integral equation for G can be written as [8] :

$$\begin{aligned} G(P,Q;\vec{x},\vec{x}';E) &= G_0(P,Q;\vec{x},\vec{x}';E) - i\sum_{\Lambda=\sigma,\omega} g_\Lambda^2 \int d^3y d^3y' \\ &\times G_0(P,\Gamma^\Lambda;\vec{x},\vec{y};E) D_{(\Lambda)}(\vec{y}-\vec{y}';E) G(\Gamma_\Lambda,Q;\vec{y}',\vec{x}';E) \ , \end{aligned} \tag{16}$$

where g_σ, g_ω are the coupling constants, $D_{(\sigma)}$ and $D_{(\omega)}$ are the meson propagators in coordinate representation, Γ^σ is the unit operator $\mathbf{1}$ and $\Gamma^\omega = \gamma^\mu (\mu = 0,1,2,3)$.

The RRPA polarization operator $\Pi(P,Q;\vec{k},\vec{k}';E)$ is defined in the same way as the unperturbed Π_0 of eq.(11). From eq.(16), we can easily deduce the integral equation obeyed by Π. Pictorially, the RRPA equation for Π, in the present ring approximation, is represented in Fig.2. If we make a multipole expansion of Π similar to that of eq.(12) we find that the

multipole components $\Pi^{(L)}$ must satisfy the one-dimensional integral equation :

$$\begin{aligned}\Pi^{(L)+}(P,Q;k,k';E) &= \Pi_0^{(L)+}(P,Q;k,k';E) - \int k"^2 dk" \\ &\times \left\{ g_\sigma^2 \Pi_0^{(L)}(P,\mathbf{1};k,k";E) D_{(\sigma)}(k",E) \Pi^{(L)}(\mathbf{1},Q;k",k';E) \right. \\ &\left. + g_\omega^2 \Pi_0^{(L)}(P,\gamma^\mu;k,k";E) D_{(\omega)}(k",E) \Pi^{(L)}(\gamma_\mu,Q;k",k';E) \right\} .\end{aligned} \tag{17}$$

In this equation, the meson propagators $D_{(\sigma)}$ and $D_{(\omega)}$ are given by :

$$\begin{aligned} D_{(\sigma)}(\underline{k}") &= \frac{1}{(2\pi)^3} \frac{1}{\underline{k}"^2 - m_\sigma^2 + i\varepsilon} \\ D_{(\omega)}(\underline{k}') &= -\frac{1}{(2\pi)^3} \frac{1}{\underline{k}"^2 - m_\omega^2 + i\varepsilon} , \end{aligned} \tag{18}$$

where m_σ and m_ω are the meson masses, and $\underline{k}"^2 = E^2 - \vec{k}"^2$.

Eq.(17), together with the explicit expression (15) for $\Pi_0^{(L)}$, form the basis of our numerical study. Once eq.(17) is solved, the value of the RRPA response function at momentum transfer k and excitation energy E is obtained as in the unperturbed case (see eq.(13)).

3 Calculations of response functions

The above scheme has been applied to the calculation of isoscalar response functions of various multipolarities for ^{12}C , ^{16}O , ^{40}Ca and ^{90}Zr nuclei. Our aim is to study whether the relativistic model can predict correctly the energies and transition strengths of giant multipole resonances. The formulas of the previous section are valid for the general case of finite momentum transfer k (e.g., the quasi-elastic peak region of the nuclear response), but we restrict ourselves in the present work to the limiting case $k \to 0$ as it is done in most

non-relativistic RPA calculations. Thus, our choice of operators P_L and Q_L (see, e.g., eq.(15)) is $P_L = Q_L = x^L Y_{L0}(\hat{x})$ if $L \neq 0$ and $x^2 Y_{00}$ if $L = 0$.

The Hartree self-energy $\sum(\vec{x})$ is calculated self-consistently by solving the Dirac-Hartree equation in coordinate space [2]. In this work, we have used the coupling constants of ref.[11] which were adjusted in the Hartree (i.e., mean field) approximation. Besides σ and ω mesons, this model includes a ρ meson which plays a role only in $N \neq Z$ nuclei at the Hartree level but plays no role in the p-h interaction for isoscalar channels. In solving eq.(17), we have used a static approximation by dropping the E-dependence in the meson propagators, since the energy in the giant resonance region is much smaller than the meson masses. We have checked in a few cases that the results were not affected when this energy dependence was kept.

The single particle spectrum is discretized by diagonalizing eq.(1) on a basis of harmonic oscillator functions. The truly bound states (both Fermi and Dirac states) are stable with respect to the choice of this basis as long as the basis vectors span a large enough space. On the other hand, the positions of unbound states depend strongly on the basis space. Thus, calculated response functions may contain, besides true collective states, some unphysical structures which are due to our approximate handling of the continuum. This inconvenience can be diminished to a large extent, firstly by performing an appropriate energy average of the response function which will render it a continuous function of excitation energy, and secondly by an optimum choice of harmonic oscillator space. The energy averaging is done in the usual

way by replacing all real energies E in denominators by complex ones $E + i\Delta/2$, a procedure which corresponds to a folding of the response function with a Lorentzian factor of width Δ [3]. Most of the numerical results discussed in the next section have been obtained with $\Delta =$ 5 MeV, a value sufficiently large to smooth out the unphysical structures while leaving the collective states visible. Some of the energy-weighted moments have been calculated by using a smaller Δ ($\Delta = 2$ MeV) to diminish the influence of the Lorentzian tail. The harmonic oscillator space is spanned by $N_0 = 12$ states for each set of individual quantum numbers, the harmonic oscillator constant being $b = 1.8$ fm. In building the $p-h$ configuration space, we have kept only states lying within some energy cut-off range ($E_F^{\max} = M + 100$ MeV for Fermi states, $E_D^{\min} = -M + 200$ MeV for Dirac states, unless specified otherwise). We have checked that, by varying the values of $N_0, b, E_F^{\max}$ and $E_D^{\min}$ within reasonable limits, the main features of the results are essentially unchanged.

Concerning the role of Dirac states, i.e. of Pauli-violating $N\bar{N}$ excitations, we find that they affect little the description of giant resonances in the $(2-3)\hbar\omega$ energy region. Therefore, it is sufficient to calculate the multipole response functions by including only the G_0^+ term of eq.(10), i.e. the $\Pi_0^{(L)}$ terms in eq.(17) can be replaced by $\Pi_0^{(L)+}$. Finally, the integral equation (17) is numerically solved in k-space on a grid of 30 mesh points in steps of 0.25 fm^{-1}.

4 Results and discussion

4.1 $L = 0$ states

The RRPA response functions $R^{(L)}(E)$ for the isoscalar monopole mode (breathing mode) are shown in Fig.3 for the three nuclei ^{16}O , ^{40}Ca and ^{90}Zr . This mode is interesting because it reflects to some extent the compressibility of nuclear matter, although the relationship is somewhat indirect due to important surface effects.

In the two light nuclei (^{16}O and ^{40}Ca) the monopole strength if distributed over an energy interval considerably wider than the averaging width $\Delta = 5$ MeV. If we look at the full width at half-maximum (FWHM), it is of the order of 15 MeV in both cases. Thus, the model does not predict here the existence of a typical giant resonance containing a large fraction of the total strength within a small energy interval. This particular feature of the isoscalar monopole strength in light nuclei is also found in non relativistic RPA models. For instance, RPA calculations performed with Skyrme interactions and where continuum effects are included (i.e., without energy averaging) show that the monopole strength in ^{40}Ca is spread over 10 MeV [12]. The situation becomes somewhat different when we go to the heavier nucleus ^{90}Zr where the value of FWHM is 9 MeV, indicating that the natural width (escape width and Landau damping) is of the order of 4 MeV. For comparison, we recall that the continuum-RPA calculation of ref.[12] gives 2.6 MeV for the FWHM in ^{90}Zr . Thus, both relativistic and non-relativistic RPA models find the same tendency that the breathing

mode becomes more collective when one goes to heavier nuclei.

The energetics of the breathing mode is shown in Table 1. The first row lists the peak energies $E_{\rm peak}$ of Fig.3. In ^{40}Ca and ^{90}Zr , they can be compared with the values of $E_{\rm peak}$ obtained in ref.[12]. Because the strength distributions are broad, we also indicate the various mean energies :

$$\begin{aligned} \bar{E} &\equiv m_1/m_0 \ , \\ E_k &\equiv (m_k/m_{k-2})^{1/2} \ , \quad k = 1,3 \end{aligned} \tag{19}$$

where

$$m_k \equiv \int_0^{E\max} R^{(L)}(E') E'^k dE' \ , \tag{20}$$

$E_{\rm max}$ being the maximum excitation energy (about 75 MeV) where the present calculations were carried out. One can see that our calculated energies are systematically larger than those of ref. [12] which were obtained with a Skyrme interaction (SGII) adjusted to give a nuclear matter compression modulus $K = 217$ MeV. Note that the SGII interaction predicts the correct monopole energy in ^{208}Pb [12].

The too high monopole energies of the present model are to be expected since the corresponding compression modulus of nuclear matter is $K = 545$ MeV [11], i.e. considerably larger than the value of SGII. It is even surprising that the discrepancy between the two models is so small. Recently, Nishizaki et al. [7] have given an estimate of monopole energies in the (σ,ω) model using a local Lorentz boost and scaling method. They find the following

result :

$$(\hbar\omega)_M = \left[\frac{K}{\epsilon_F < r^2 >}\right]^{1/2} , \tag{21}$$

where ϵ_F is the Fermi energy in nuclear matter and $< r^2 >$ the mean square radius. Approximating ϵ_F by M and $< r^2 >$ by $\frac{3}{5}(1.2)^2 A^{2/3} fm^2$ one finds, with the present value of K :

$$(\hbar\omega)_M \simeq 160 A^{-1/3} MeV , \tag{22}$$

i.e., about twice the experimental systematics. In Table 1, one can see that the DHRPA model leads to energies substantially smaller than the estimate (22). Clearly, monopole energies in finite nuclei are not only governed by bulk properties like K, and surface effects are quite important for lowering monopole resonance energies, especially in the (σ,ω) model. In any case, a quantitative agreement with experimental energies could probably be obtained if one includes cubic and quartic terms of the σ-field in the effective Lagrangian in order to bring down the value of K [13].

4.2 $L = 2$ states

The calculated response functions $R^{(L=2)}(E)$ for isoscalar quadrupole modes are shown in Figs.4 and 5. When low-lying discrete states are present (in $L = 2$, 3 and 4 cases) we have subtracted out their contributions before drawing $R^{(L)}$, for the clarity of the figures. In ^{12}C where the calculation was done with a single-particle cut-off $E_F^{max} = M + 40$MeV, the strength distribution is very broad and exhibits no pronounced giant resonance behaviour.

Below particle emission threshold ($E_{threshold}$ = 12.75 MeV) there is a strong bound state near 5 MeV and built mainly on truly bound configurations like $(1p3/2^{-1}\ 1p1/2)$. Such a low-lying RRPA bound state of course does not exists in ^{16}O , where the quadrupole response shows a well marked peak around E_{peak} = 24 MeV. A similar situation occurs in ^{40}Ca (see Fig.5). The shape of the quadrupole response in ^{16}O and ^{40}Ca is very similar to that given by continuum-RPA calculations with Skyrme forces [5,14], with the difference that the present model predicts slightly higher quadrupole resonance energies. In Fig.5 is also shown the Hartree response $R_0^{(L=2)}$ in ^{40}Ca , to illustrate the strong effect of residual $p-h$ interaction in producing a collective giant resonance. The case of ^{90}Zr is similar to that of ^{12}C ; besides a strong state in the continuum region with a relatively narrow width, there is another low-lying collective state at 7 MeV and containing 35 % of the total quadrupole strength. This state is above proton emission threshold but below neutron threshold, and consequently it must have a very small intrinsic width which we have not tried to estimate accurately by our averaging procedure.

The energetics of the quadrupole mode is shown in Table 2. The peak energy E_{peak} decreases steadily when one goes from ^{12}C to ^{90}Zr , and this is accompanied by a narrowing of the giant resonance as indicated by the values of FWHM. Since we have used an averaging width Δ = 5 MeV, one can see that the intrinsic width of the quadrupole resonance in ^{90}Zr is probably of the order of 1 MeV. In Table 2 we have also indicated the peak energies in ^{12}C and ^{40}Ca coming from continuum-RPA calculations performed with the Skyrme interaction

SIII [5,14]. These calculations give FWHM values of 1.7 MeV and 1. MeV in ^{12}C and ^{40}Ca , respectively. The various energies $\bar{E}$, E_1 and E_3 defined in eq.(19) are shown in Table 2. In ^{12}C and ^{90}Zr the centroid energies $\bar{E}$ are shifted to lower values because of the presence of a low lying quadrupole state, in contrast to the ^{16}O and ^{40}Ca cases.

In ref.[7] an estimate of quadrupole energies in the (σ,ω) model has been derived, using again a local Lorentz boost and scaling method as in the monopole case. The result is :

$$(\hbar\omega)_Q = \left[\frac{6p_F^2}{5E_F^*\epsilon_F < r^2 >}\right]^{1/2} \simeq 90A^{-1/3} \text{ MeV} , \tag{23}$$

where p_F is the Fermi momentum, and $E_F^* = (p_F^2 + M^{*2})^{1/2}$ with M^* being the relativistic effective mass. The numerical estimates shown in Table 2 are obtained with the inputs of ref.[11]. Except for the lighter nuclei ^{12}C and ^{16}O , the agreement between $(\hbar\omega)_Q$ and our calculated values, especially for E_3 energies, is satisfactory. We note, however, that $(\hbar\omega)_Q$ is always somewhat larger than E_{peak}. Even though the estimate (23) is almost 50 % above experimental systematics, the calculated values of E_{peak} are not so much off as one can see by comparing with the SIII energies (see row (c) of Table 2). A moderate increase of M^* from its present value of 0.541 would be needed in order to come close to experimental energies.

4.3 Higher multipole states

The same calculational scheme has been applied to the case of $L = 3$ and $L = 4$ isoscalar modes. In Fig.6 are shown the response functions $R^{(L=3)}$ in ^{16}O and ^{90}Zr . Both strength

distributions exhibit a strong collective state at low energy. This state contains 1/3 of the total $L = 3$ strength in ^{16}O , and about 1/2 in ^{90}Zr . The rest of the strength is very widely spread up to 60 MeV in the case of ^{16}O , where the oscillations are probably due to the procedure used here to discretize the continuum. in ^{90}Zr , a resonance structure appears around 32 MeV, but there is also a substantial background from 10 to 30 MeV.

An example of $L = 4$ response functions is displayed in Fig.7. In ^{40}Ca there is a well-marked peak at $E_{peak} = 17$ MeV and a large background persisting up to 75 MeV. We find that this background is very close to the Hartree strength distribution for excitation energies above 20 MeV. The overall aspect of the $L = 4$ response in ^{40}Ca is similar to that found in non-relativistic continuum-RPA calculations [5]. In ^{90}Zr the most apparent structures consist of a low-lying state at 8 MeV, two resonances at 12 MeV and 20 MeV and a far extending tail. Again, the oscillations in the 35-45 MeV region may be attributed to the continuum discretization procedure.

In general, these calculations show that, for $L > 2$, the collectivity is much less pronounced and the multipole strength tends to be distributed over a wide energy range.

5 Conclusion

We have applied a relativistic RPA approach to the study of giant resonances in finite nuclei. The present model is consistent in the sense that the same effective Lagrangian determines self-consistently the Dirac-Hartree single-particle spectrum and also the p-h interaction.

Thus, there are no more free parameters once the coupling constants have been adjusted on nuclear matter and ground state properties.

We have restricted ourselves to the ring approximation, without exchange contributions in the interaction vertices. This approximation is consistent with the Dirac-Hartree approximation used for determining the starting effective Lagrangian. The omission of exchange (Fock) terms results in a renormalization of coupling constants for the isoscalar mesons [2], but it leaves the couplings of isovector mesons rather badly determined. Indeed, in the Dirac-Hartree approximation, the ρ meson contributes only in $N \neq Z$ systems while the π meson does not contribute at all. Therefore, the ring approximation may be acceptable for isoscalar modes, but a study of isovector giant resonances would require an RPA calculation where exchange interaction vertices are also included and where π - and ρ -coupling constants are determined from a Dirac-Hartree-Fock model of nuclear ground states [2].

In the case of isoscalar monopole resonances, we find that the resonance energy is not well defined in light nuclei (^{16}O , ^{40}Ca), but the breathing mode appears strongly in ^{90}Zr . A detailed comparison with non-relativistic RPA results shows that the relativistic model predicts too high energies, but much less than the large discrepancy that one might guess by looking only at the value of the compression modulus (K= 545 MeV) of the present model. The prediction (21) based on a scaling method [7] is also seen to be largely overestimating the present results. It seems quite possible to obtain reasonably good monopole energies in finite nuclei if one lowers moderately the compression modulus from its present value, for

instance by adding σ^3 and σ^4 terms to the Lagrangian.

The isoscalar quadrupole resonances appear as collective states in all nuclei. The residual interaction is strongly attractive in this model and shifts the RPA strength several MeV below the unperturbed strength. The calculated quadrupole energies are higher than those predicted by non-relativistic RPA calculations which more or less agree with the data. One may relate this defect to the rather small value of the effective mass M^* . Other effective Lagrangians with larger values for M^* [2] could perhaps improve the prediction of quadrupole energies. The comparison of our results with the prediction (23) obtained by the scaling method of ref.[7] is satisfactory if one does not consider nuclei lighter than ^{40}Ca and if one identifies the quantity $(\hbar\omega)_Q$ of eq.(23) with our E_3 energy.

It would be interesting to explore further the properties of RPA states in the relativistic approach. On the one hand, our discretization and averaging procedure has the advantage of rendering numerical calculations rather fast, but it has the disadvantage of not treating correctly continuum effects. It is possible to improve on this point by using a representation of the single-particle propagator G_H in terms of two linearly independent solutions of the Dirac equation, as it was done for instance by Wehrberger and Beck [15]. On the other hand, the relativistic model should also be applied to the study of isovector giant resonances, where π and ρ mesons should play a prominent role. Another question of interest is that raised by Auerbach et al. [16] who argue about the existence of discrete $N\bar{N}$ states embedded in the continuum. These states are described by the $G_F G_F$ terms neglected in the present work,

and our formalism could be used to study these $N\bar{N}$ excitations and their modifications due to residual interaction.

References

[1] B.D. Serot and J.D. Walecka, Adv. Nucl. Phys. **16**, 1 (1986)

[2] A. Bouyssy, J.F. Mathiot, Nguyen Van Giai and S. Marcos, Phys. Rev. **C36**, 380 (1987)

[3] G.F. Bertsch and S.F. Tsai, Phys. Rep. **18C**, 127 (1975)

[4] J. Dechargé and L. Šips, Nucl. Phys. **A407**, 1 (1983)

[5] Nguyen Van Giai, Suppl. Prog. Theor. Phys. **74-75**, 330 (1983)

[6] O. Bohigas, A.M. Lane and J. Martorell, Phys. Rep. **51**, 267 (1979)

[7] S. Nishizaki, H. Kurasawa and T. Suzuki, Nucl. Phys. **A462**, 687 (1987)

[8] H. Kurasawa and T. Suzuki, Nucl. Phys. **A445**, 685 (1985)

[9] S.A. Chin, Ann. of Phys. (N.Y.) **108** , 301 (1977)

[10] A.L. Fetter and J.D. Walecka, Quantum Theory of Many-Particle Systems, McGraw-Hill (New York) 1971.

[11] C.J. Horowitz and B.D. Serot, Nucl. Phys. **A368**, 503 (1981)

[12] Nguyen Van Giai and H. Sagawa, Nucl. Phys. **A371**, 1 (1981)

[13] A. Bouyssy, S. Marcos and Pham Van Thieu, Nucl. Phys. **A422**, 541 (1984)

[14] K.F. Liu and Nguyen Van Giai, Phys. Lett. **65B**, 23 (1976)

[15] K. Wehrberger and F. Beck, preprint IKDA 88/1, Darmstadt

[16] N. Auerbach, A.S. Goldhaber, M.B. Johnson, L.D. Miller and A. Picklesimer, Phys. Lett. **B182**, 221 (1986)

Table captions

Table 1 : Calculated monopole energies (in MeV) in finite nuclei. The quantities $E_{peak}, E_1, \bar{E}$ and E_3 are explained in the text, the bottom line is the estimate (22). Rows (a) correspond to this work, (b) to ref. [12].

Table 2 : Same as Table 1, for quadrupole energies. The quantity $(\hbar\omega)_Q$ is the estimate (23), FWHM shows the width of the main peak. Row (a) corresponds to this work, (c) to refs.[5,14].

Nucleus		^{16}O	^{40}Ca	^{90}Zr
E_{peak}	(a)	23.	25.	21.5
	(b)		23.	18.5
E_1	(a)	22.9	22.9	21.4
$\bar{E}$	(a)	24.5	24.3	22.4
	(b)		22.7	19.5
E_3	(a)	29.2	28.5	25.5
$(\hbar\omega)_M$		63.5	46.8	35.7

Table 1

Nucleus		^{12}C	^{16}O	^{40}Ca	^{90}Zr
E_{peak}	(a)	25.5	25.	19.5	16.5
	(c)		20.5	17	
E_1		11.8	24.3	20	12.4
$\bar{E}$		18.1	25.3	20.8	14.4
E_3		30.9	28.1	23.3	19.2
$(\hbar\omega)_Q$		39.2	35.6	26.2	20
FWHM		13.	9.2	7.4	6.1

Table 2

Figure captions

Figure 1 : The Dirac-Hartree single-particle spectrum.

Figure 2 : Diagrammatic representation of the RRPA equation (17).

Figure 3 : Monopole response functions $R^{(L=0)}(E)$ (in fm^4 MeV^{-1}) as functions of excitation energy E (in MeV).

Figure 4 : Quadrupole response functions $R^{(L=2)}(E)$ (in fm^4 MeV^{-1}) in ^{12}C and ^{16}O . The arrow indicates the position of a low-lying bound state in ^{12}C .

Figure 5 : Same as Fig.4, for ^{40}Ca and ^{90}Zr . The dotted curve shows the Hartree response in ^{40}Ca . The arrow indicates the position of a low-lying bound state in ^{90}Zr .

Figure 6 : $L = 3$ response functions (in fm^6 MeV^{-1}) in ^{16}O and ^{90}Zr . Arrows indicate low-lying states.

Figure 7 : $L = 4$ response functions (in fm^8 MeV^{-1}) in ^{40}Ca and ^{90}Zr . The arrow indicates a low-lying state in ^{90}Zr . The ^{90}Zr curve corresponds to $\Delta = 2$ MeV.

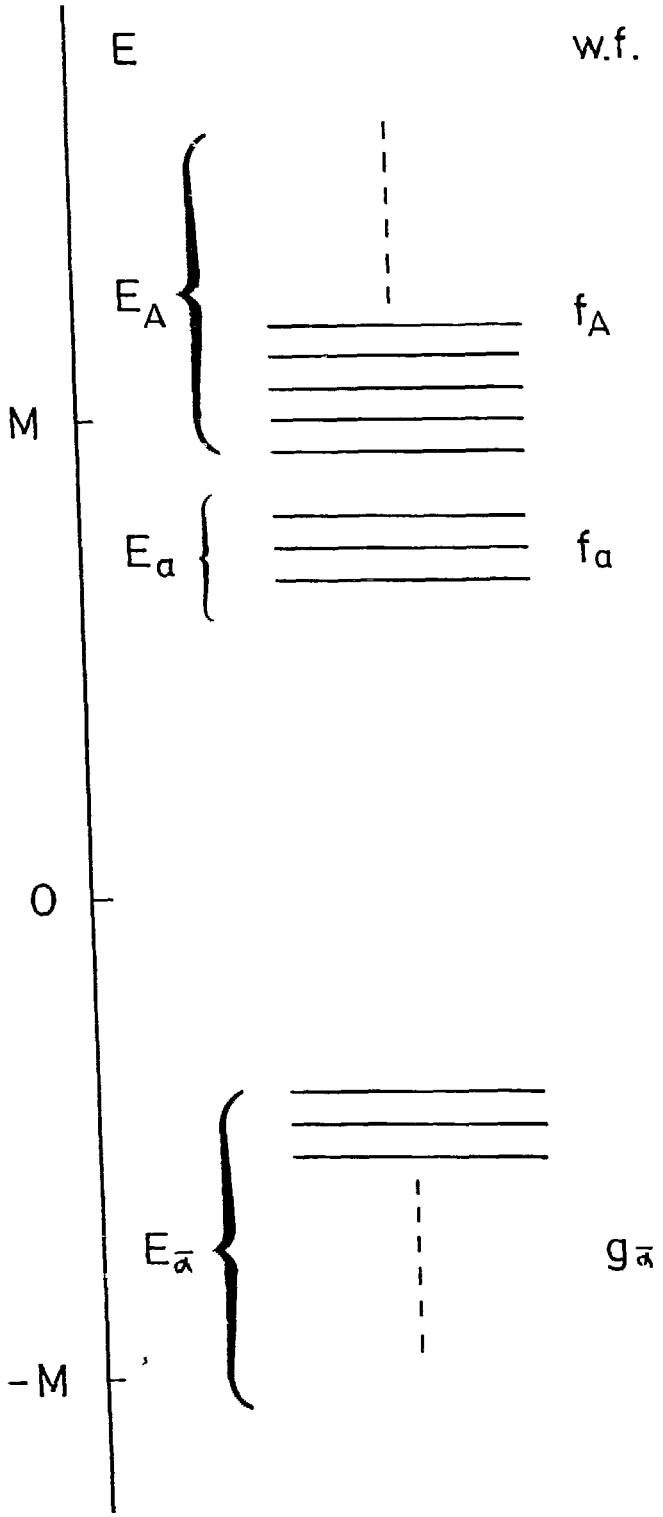

Fig. 1

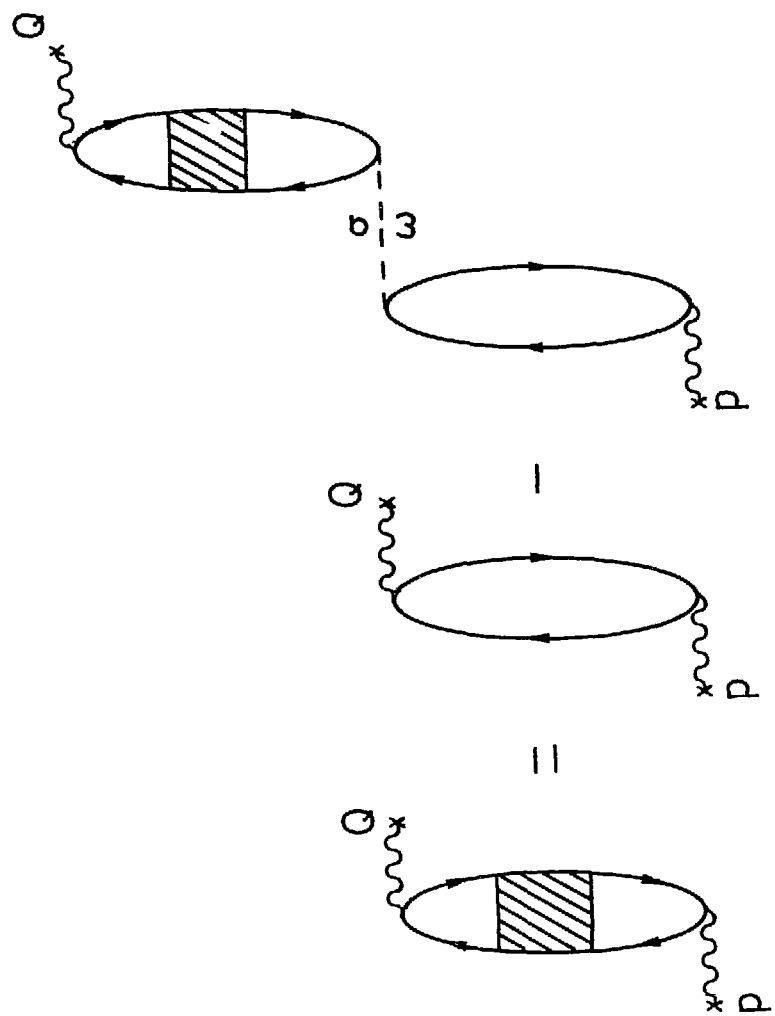
Q
σ 3
p
I
Q
p
II
Q
p

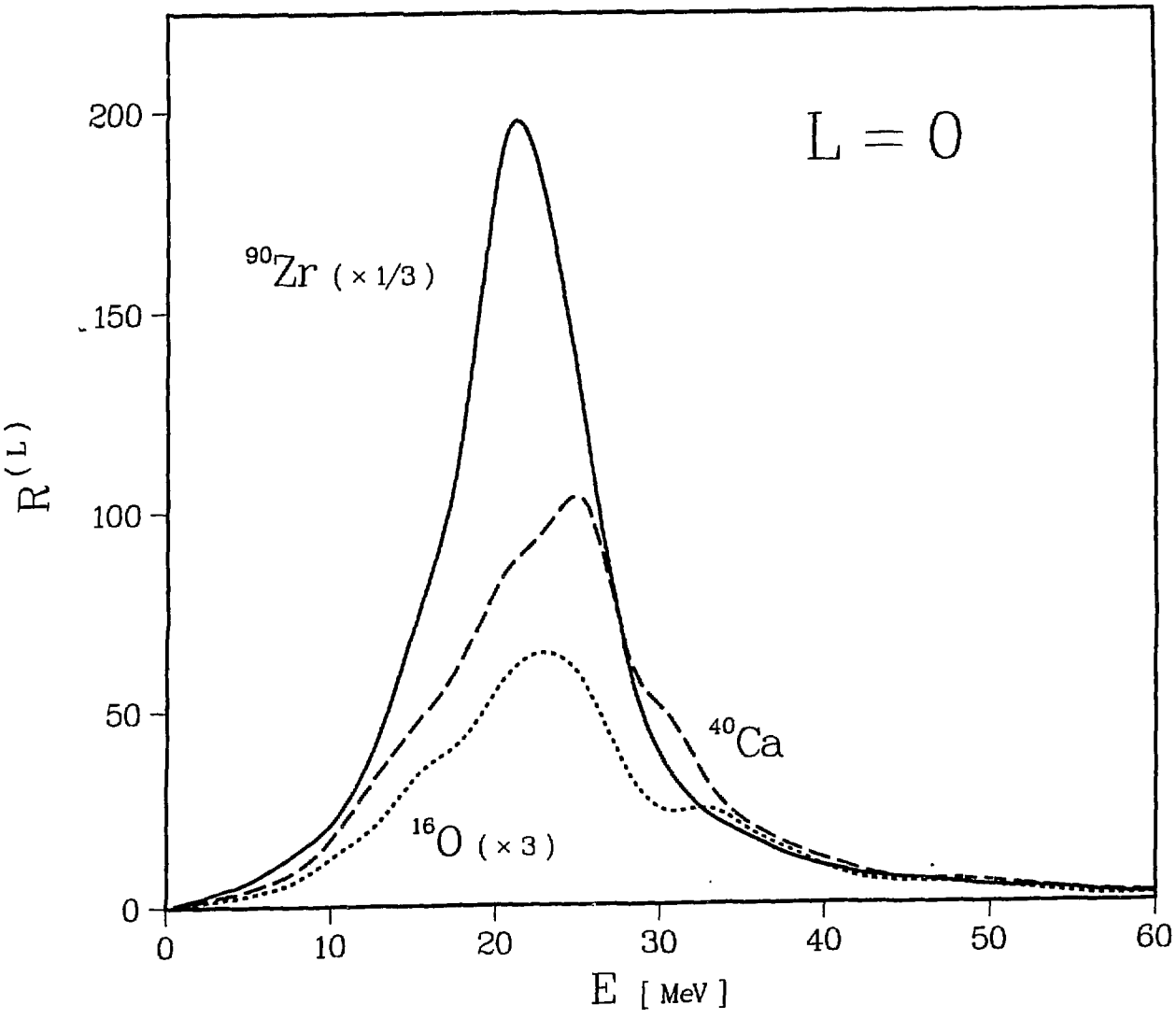

Fig. 3

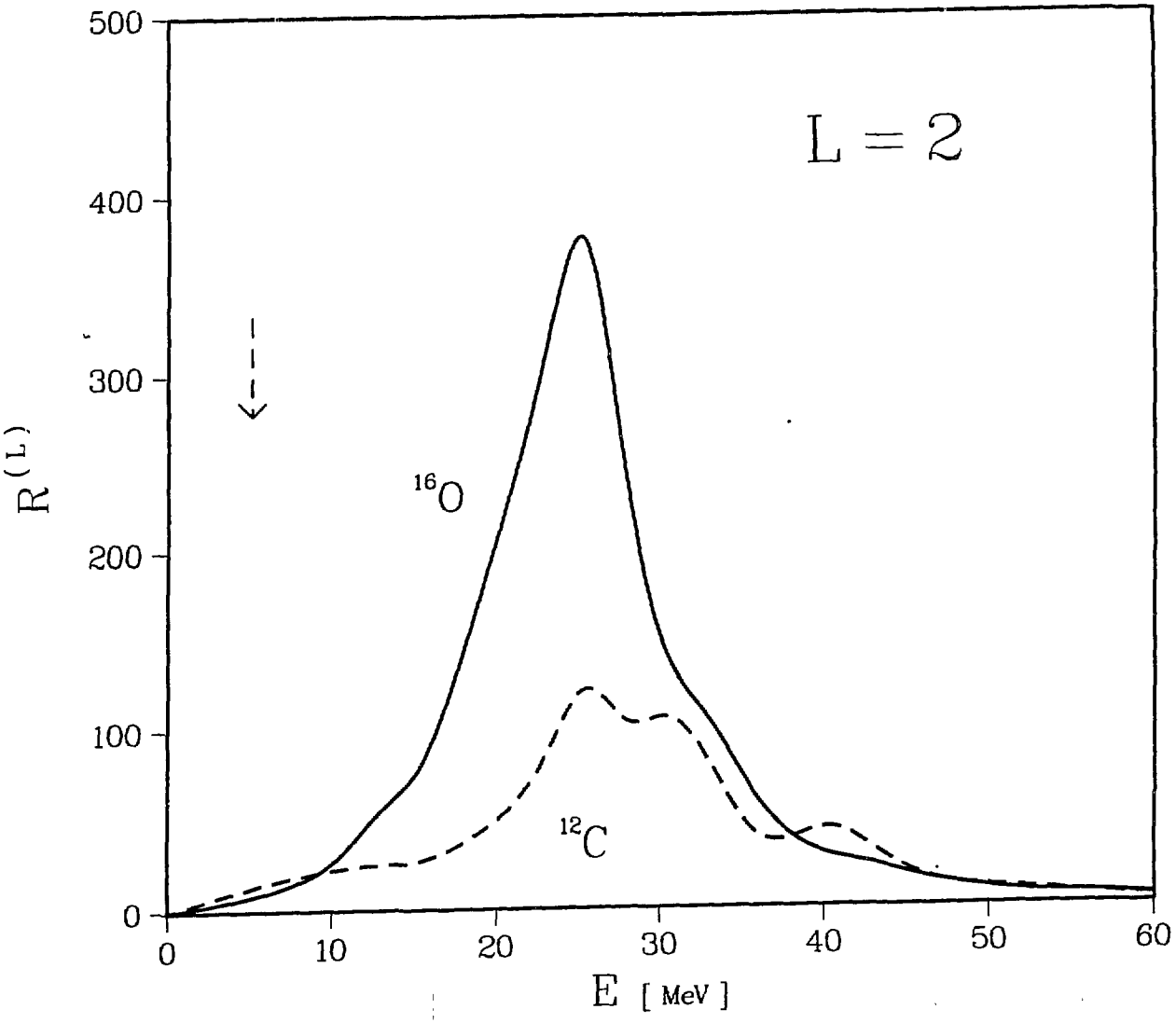
L = 2
^{16}O
^{12}C
$R^{(L)}$
E [MeV]
0
100
200
300
400
500
0
10
20
30
40
50
60

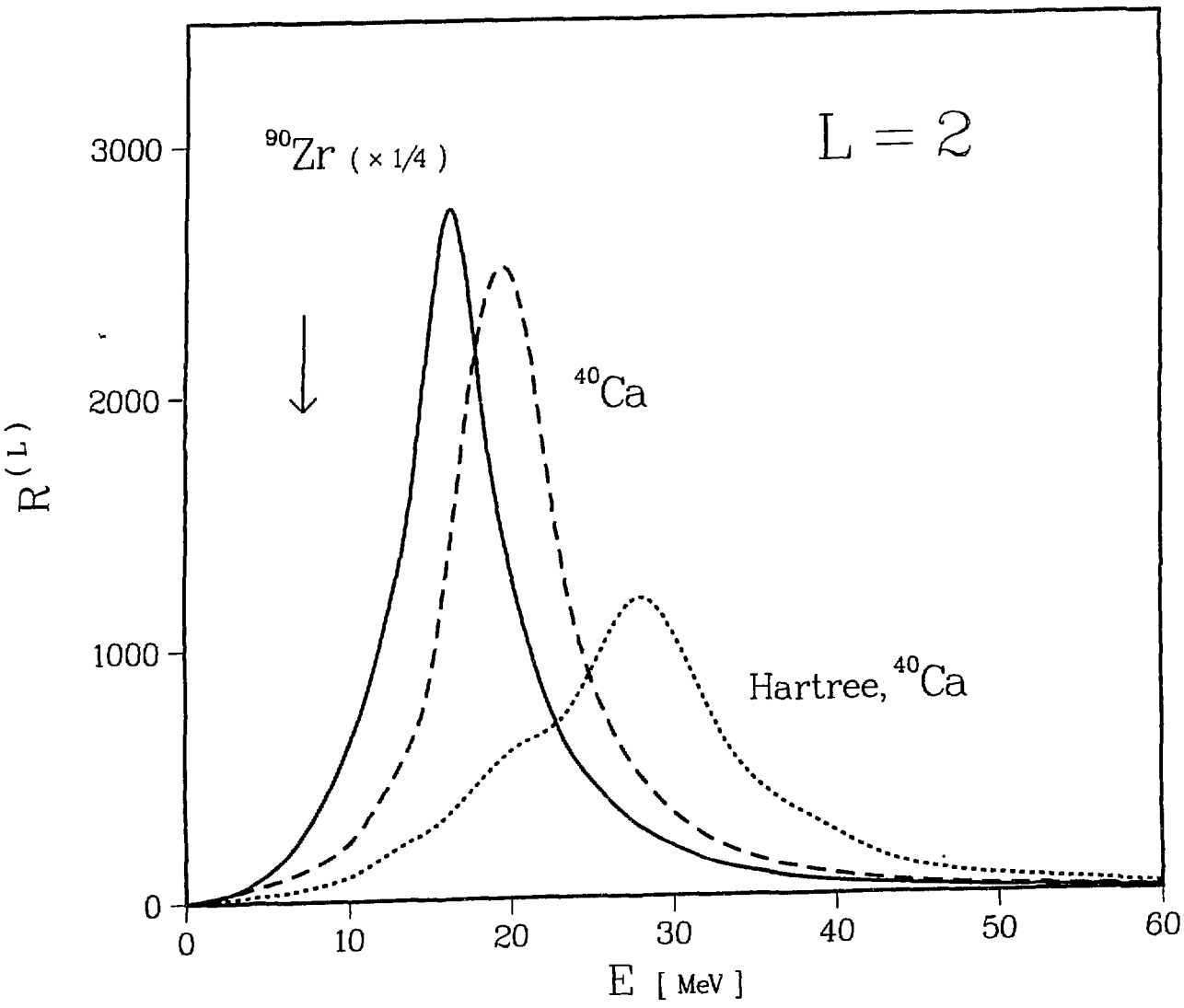
L = 2
^{90}Zr (× 1/4)
^{40}Ca
Hartree, ^{40}Ca
R(L)
E [MeV]
0
1000
2000
3000
0
10
20
30
40
50
60

Fig. 5

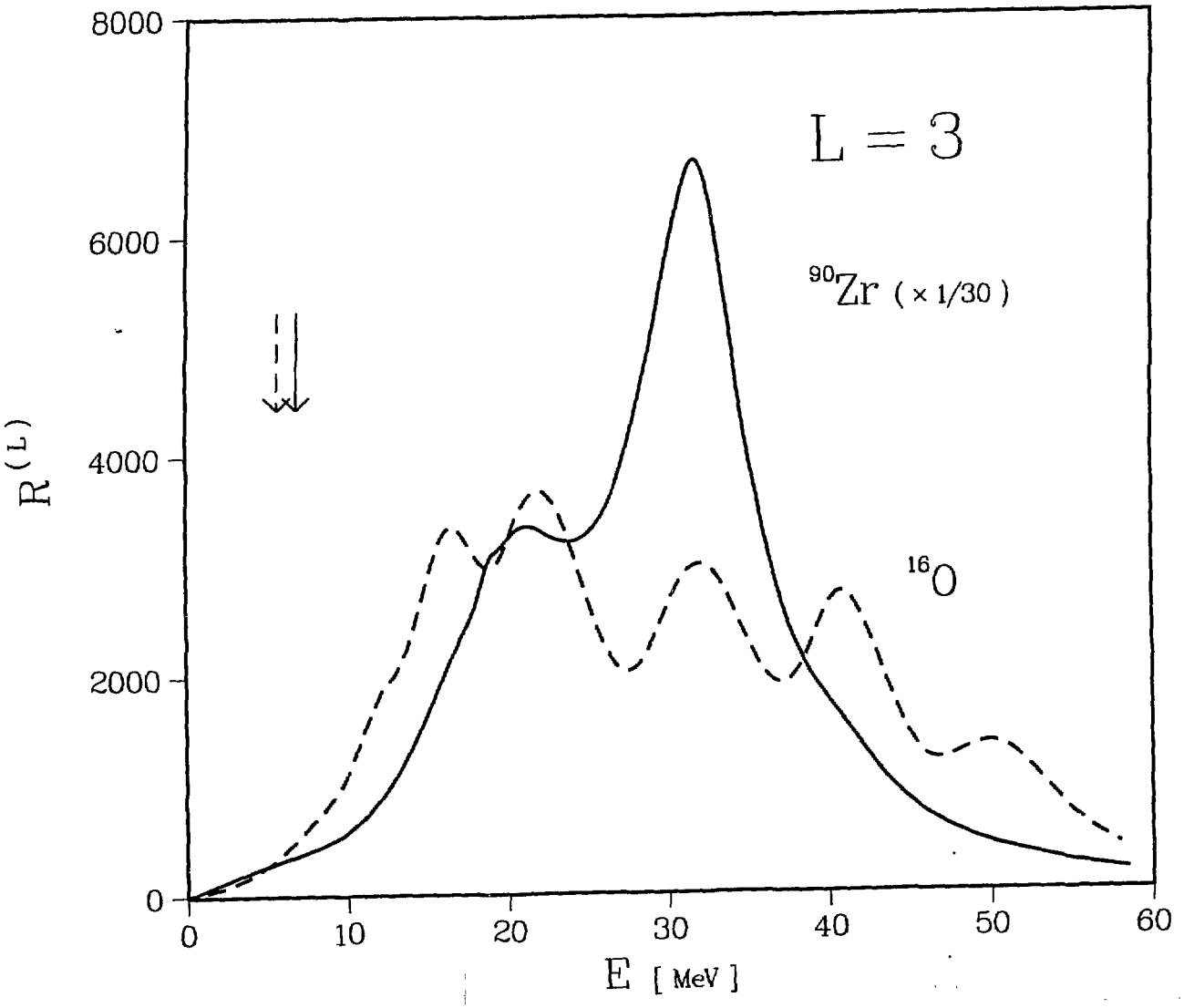

Fi . 6

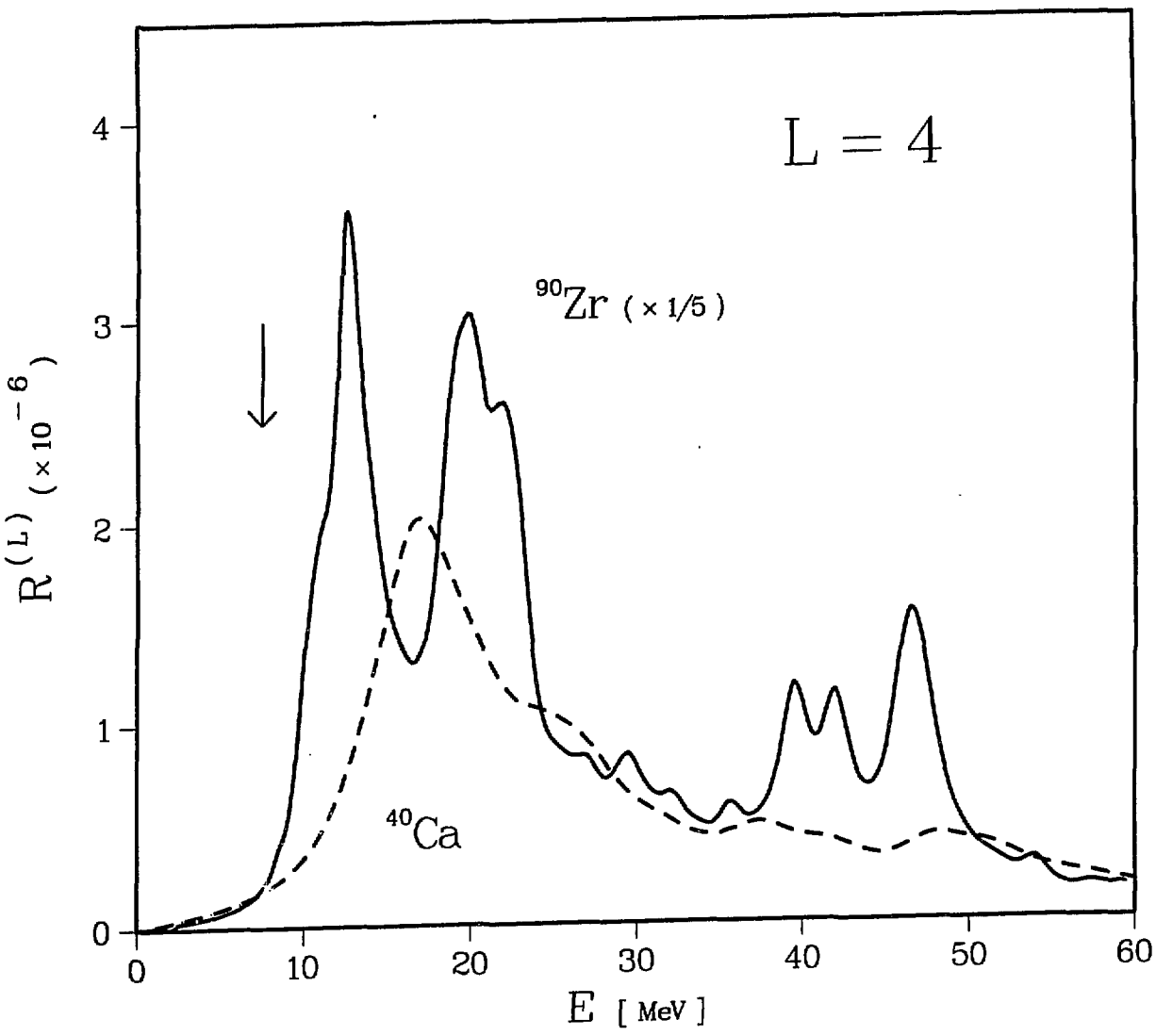

Fig. 7